A TRIANGULAR THIN SHELL FINITE ELEMENT
FOR LAMINATED GENERAL SHELLS

S.Sridhara Murthy, Scientist, Structures Division
National Aeronautical Laboratory
BANGALORE 560 017

ABSTRACT

The problems associated with the finite element analysis of thin shell structures are discussed with the objective of developing a simple and efficient thin shell finite element. It has been pointed out that the difficulties in the formulation of thin shell elements stem from the need for satisfaction of the interelement normal slope continuity and the rigid body displacement condition by the displacement trial functions. These difficultites have been surmounted by recourse to the discrete Kirchhoff theory (DKT) approach and an isoparametric representation of the shell middle surface.

A three node curved triangular element with simple nodal connections has been developed wherein the displacement and rotation components are independently interpolated by complete cubic and quadratic polynomials respectively. The rigid body displacement condition is satisfied by isoparametric interpolation of the shell geometry within an element. A convergence to the thin shell solution is achieved by enforcement of the Kirchhoff hypothesis at a discrete number of points in the the element. A detailed numerical evaluation through a number of standard problem has been carried out. Results of application of a patch test solution to a spherical shell demonstrates the satisfactory performance of the element under limiting states of deformation.

It is concluded that the DKT approach in conjunction with the isoparametric representation results in a simple and efficient thin shell element.

A TRIANGULAR THIN SHELL FINITE ELEMENT FOR LAMINATED GENERAL SHELLS

S.Sridhara Murthy, Scientist, Structures Division
National Aeronautical Laboratory
BANGALORE 560 017

INTRODUCTION

The analysis of thin shells has been one of the sought-after applications of the finite element method. Although the research effort in this direction has been significant, the success of the method for thin shell analysis has been less t han completely satisfactory, and it continues to attract the research attention.

There is a considerable interest in the development of simple and efficient curved triangular conforming finite elements based on thin shell theories using displacement approach. The choice of shell theory and the interpolation of displacement field are two of the important issues in the development of thin shell finite elements.

The strain energy of a shell is usually calculated by employing one of the classical shell theories. Since the beginning, due to their well established nature, thin shell theories based on Kirchhoff hypothesis have formed the basis for the formulation of plate and shell elements. The displacement trial functions should satisfy certain conditions in order to have theoretical assurance of convergence of the numerical solution. The important among these are: (a) the satisfaction of inter-element continuity of the displacement and its derivatives upto one order less than that of the highest in the associated functions to be minimised, and (b) the satisfaction of the condition of zero strain energy under rigid body displacements.

The conformity condition, in conjunction with the Principle of Minimum Potential Energy (PMPE), demands the continutiy of the normal slope across the inter-element boundaries for a conforming plate or shell element. The difficulties in forming a Kirchhoff-theory conforming triangular plate or shell element with simple nodal connections are well known in the literature [1]. Thus, the adherence to the Kirchhoff hypothesis has led to the difficulties associated with the C^1-continuous interpolation over the triangle.

The above difficulty prompted the development of plate and shell elements based on shell theories which relax the Kirchhoff hypothesis, and led to the so called "Discrete Kirchhoff Theory" (DKT) approach. The development of this approach can be traced in Reference[2]. The DKT approach has been highly successful for plate elements [3], and a few applications to curved thin shell elements have also appeared in the literature [4].

In the DKT approach, the bending energy is calculated from independently- assumed normal rotations. To force the convergence of the solution to that of the classical theory, "Kirchhoff hypothesis" type constraints are enforced at a discrete number of points in the element. Thus the normal rotations are eliminated in terms of the derivatives of the reference surface displacements and one arrives at a conforming element with conventional degrees of freedom.

The displacement trial functions must also include an accurate representation of the rigid body modes for an acceptable rate of convergence [5]. Noncompliance with this condition, however, does not preclude convergence to the correct solution [6], although the convergence rate may not be acceptable from practical considerations. Also, in problems where "rigid body type" displacements are considerable, significant errors due to the straining in the rigid body modes will be introduced.

Some of the earlier thin shell elements (e.g.[7,8]) did not contain an explicit representation of the rigid body modes. It was argued, however, that the higher order polynomial representations for the displacements would result in a good approximation for the rigid body modes which contain trigonometric functions of the curvilinear coordinates [8]. Later, it was observed by Morris [9] that the use of higher order polynomials does not remove the rigid body errors, but can only reduce their influence. Notwithstanding, an exact representation of the rigid body modes can be achieved by recourse to isoparametric representation of the shell middle surface within an element. The SHEBA element of Argyris and

Scharpf [10], and the triangular element of Dupuis[5] are some of the earlier thin shell elements wherein an explicit representation of the rigid body modes are included. The more recent thin shell element due to Wu[11,12], closely following the theoretical basis of SHEBA element, is another example of this class. The above elements are, however, based on shell theories which accept the Kirchhoff hypothesis in one form or another.

The SHEBA element satisfies the conformity condition by recourse to quintic polynomials for all the displacement components, with second order derivatives as nodal quantities. The element due to Dupuis[5] uses cubic shape functions with three rational polynomials for conforming interpolation of all the displacement components. The lack of extensive numerical comparisons, and the high-order numerical integration required for the rational polynomials has made this element less attractive for practical applications.

The shell element due to Wu[12] closely follows the theoretical basis of SHEBA element, but uses the cubic interpolation scheme of Birkhoff and Mansfield [13]. The latter scheme uses nine cubic polynomial shape functions and three singular shape functions in natural area coordinates. To alleviate the difficulties associated with the singular second-order derivatives of the rational polynomials, a substitute second-order derivatives similar to those used by Irons and Razzaque[14,15] have been used. Extensive results presented show the accuracy of the element for various classes of shells [12]. However, the element stiffness matrix has a rank deficiency of two due to the lack of linear independence in the choice of the substitute shape functions. For linear buckling and geometrically nonlinear problems, this deficiency of the energy in the global level may lead to undesirable flexibility [16].

As pointed out earlier, a few thin shell elements using DKT approach have appeared in the literature. Dhatt [17] presented a twenty seven degrees of freedom element which is essentially a shallow shell element. A later presentation [18] modified it to include shallow shell rigid body conditions. A curved triangular thin shell element using the DKT approach was presented by Batoz [19]. It is based on the linear shear theory due to Wempner et al.[20], and uses cubic Hermitian polynomials for tangential displacements, and DKT representation for normal displacement resulting in a total of twenty seven degrees of freedom, nine at each corner node. The numerical results converge to those based on a deep shell theory. The shallow shell version of the element was also extended for nonlinear and stability problems [19,21]. The element formulation, however, does not contain an explicit representation of the rigid body modes.

In the present work, a new curved general thin shell finite element based on DKT approach with an explicit representation of the rigid body modes is presented. It is a three-node triangular element with twenty-seven degrees of freedom, nine at each of the corner nodes. The degrees of freedom are the tangential and normal displacement components and their first order derivatives with respect to a general curvilinear coordinates embedded on the shell middle surface. The strain energy density in the shell is calculated using the linear shear deformation theory described in a general curvilinear coordinate system due to Wempner et al.[20]. The strain-displacement relations are initially derived in terms of the displacement and rotation vectors of the shell middle surface, and are subsequently expressed in terms of the global cartesian components of these vectors to enable an isoparametric representation of the shell middle surface.

The element formulation starts with an independent interpolation of the cartesian components of the displacement and rotation vectors using complete cubic and quadratic polynomials, respectively. The rigid body displacement condition is satisfied by isoparametric interpolation of the shell geometry within an element. A convergence to the thin shell solution is achieved by enforcement of the Kirchhoff hypothesis at a discrete number of points in the element.

A detailed numerical evaluation through a number of standard problems are presented. Results for a "patch" test problem with an engineering appeal, proposed by Morley and Morris[22], demonstrates the satisfactory performance of the element under the deformation state of predominently inextensional bending together with boundary effects.

It is concluded that the DKT approach in conjunction with an isoparametric representation of the shell middle surface results in a simple and efficient thin shell finite element.

EQUATIONS FROM SHEAR DEFORMATION THEORY OF THIN SHELLS

A summary of equations from a linear shear deformation theory [20] in a general curvilinear coordinate system is presented. The strain-displacement relations are transformed into a global cartesian system to enable an isoparametric representation of the shell middle surface. Attention is focused on the derivation of an expression for the strain energy density in the shell.

Metric and curvature tensors

Indicial notation and the standard summation convention will be used for vector and tensor operations. Lower Case Latin indices $(i,j,...)$ have the range 1 to 3, and the Greek indices

$(\alpha,\beta,\gamma,...)$ have the range 1 to 2.

Figure 1 shows the geometry of a shell middle surface. The position vector to a point P on the undeformed middle surface is $\bar{R}_o(\theta^1,\theta^2)$, where θ^α = constant $(\alpha = 1,2)$ are curvilinear coordinate lines embedded on the middle surface of the shell. The position vector $\bar{R}_o$ is defined in terms of its cartesian components as

$$\bar{R}_o(\theta^1,\theta^2) = x^1(\theta^1,\theta^2)\hat{e}_1 + x^2(\theta^1,\theta^2)\hat{e}_2 + x^3(\theta^1,\theta^2)\hat{e}_3 \tag{1}$$

where $\hat{e}_i$ are cartesian base vectors, and a caret ($\wedge$) above the symbol signifies a unit vector. The position vector to an arbitrary point Q is

$$\bar{R}(\theta^1,\theta^2) = \bar{R}_o(\theta^1,\theta^2) + \theta^3\hat{a}_3 \tag{2}$$

where θ^3 is the distance along the normal to the middle surface and $\hat{a}_3$ is the unit normal vector to the middle surface. The base vectors $\bar{g}_i$ of the θ^i coordinate system follow from Eq.(2):

$$\bar{g}_\alpha = \bar{R}_{,\alpha} + \theta^3\hat{a}_{3,\alpha} \qquad \bar{g}_3 = \bar{R}_{,3} = \hat{a}_3 \tag{3}$$

where a comma denotes partial differentiation with respect to θ^α. The base vectors at the middle surface, $\bar{a}_i$, are obtaintd by setting $\theta^3 = 0$ in Eq.(3). Thus

$$\bar{a}_\alpha = \bar{R}_{o,\alpha} \qquad \bar{a}_3 = \bar{g}_3 = \hat{a}_3 \tag{4}$$

The reciprocal base vectors, $\bar{a}^i$, are defined by the relation

$$\bar{a}^i \cdot \bar{a}_j = \delta^i_j \tag{5}$$

where a period (.) denotes the dot product and δ^i_j is the Kronecker delta. The two basic vector triads are shown in Figure 1b.

The covariant and the contravariant components of the metric tensor of the θ^α coordinates are respectively given by

$$a_{\alpha\beta} = \bar{a}_\alpha \cdot \bar{a}_\beta \qquad a^{\alpha\beta} = \bar{a}^\alpha \cdot \bar{a}^\beta \tag{6}$$

These two sets of components are related as

$$a^{11} = a_{22}/a \quad a^{22} = a_{11}/a \quad a^{12} = -a_{12}/a = a^{21} \tag{7}$$

where

$$a = |a_{\alpha\beta}| = a_{11}a_{22} - (a_{12})^2 \tag{8}$$

The derivatives of the unit normal vector $\hat{a}_3$ are given by

$$\hat{a}_{3,\beta} = -b_{\alpha\beta}\,\bar{a}^{\alpha} = -b^{\alpha}_{\beta}\,\bar{a}_{\alpha} \tag{9}$$

where $b_{\alpha\beta}$ and $b^{\alpha\beta}$ are respectively the covariant and the mixed variant components of the curvature tensor of the shell middle surface.

Using Eq.(9) in Eq.(3) we obtain

$$\bar{g}_{\alpha} = \bar{a}_{\alpha} - \theta^3 b^{\beta}_{\alpha}\,\bar{a}_{\beta} \tag{10}$$

$$\bar{\bar{g}}_{\alpha} = \bar{a}_{\alpha} - \theta^3 b_{\alpha\beta}\,\bar{a}^{\beta} \tag{11}$$

The metric tensor of the spatial system, θ^i, follow from Eqs.(10)-(11):

$$g_{\alpha\beta} = \bar{g}_{\alpha}\cdot\bar{g}_{\beta} = a_{\alpha\beta} - 2\theta^3 b_{\alpha\beta} + (\theta^3)^2 b_{\alpha\gamma} b^{\gamma}_{\beta} \tag{12}$$

$$g_{\alpha 3} = 0 \tag{13}$$

Kinematics of Deformation

Figure 2 shows the deformation of a shell element. $\bar{R}_o$ is the position vector of a particle P on the undeformed middle surface, and $\bar{R}$ is that of an arbitrary point Q on the normal through P. After deformation P moves to P^*, and the corresponding position vector is $\bar{R}_o^*$. Similarly the position vector of Q is $\bar{R}^*$. If $\bar{u}$ and u^* denote the displacement vectors of the point P and Q respectively, it follows from Figure 2 that

$$\bar{R}^* = \bar{R} + \bar{u}^* \tag{14}$$

The vectors $\bar{u}$ and $\bar{u}^*$ differ by a vector $\bar{\rho}$ (see Fig.2). Assuming that normal to the middle surface remains straight with neglegible stretching, but not necessarily normal to the deformed shell, the displacement vector $\bar{\rho}$ is consequent of the rotation of the line element $P^*Q_1^*$ to P^*Q^*. This rotation of the normal can be represented by a rotation vector $\bar{\Phi}$, when the magnitude of the rotation is small. Then we can write

$$\bar{\rho} = \bar{\Phi} \times (\theta^3 \hat{a}_3) \tag{15}$$

$$\bar{u}^* = \bar{u} + \bar{\Phi} \times (\theta^3 \hat{a}_3) \tag{16}$$

where X denotes cross product. Substituting Eq.(16) in Eq.(14) we obtain

$$\bar{R}^* = \bar{R} + \bar{u} + \theta^3 \bar{\lambda} \tag{17}$$

where

$$\bar{\lambda} = \bar{\Phi} \times \hat{a}_3 \tag{18}$$

The base vectors of the deformed spatial coordinates follow from Eq.(17).

$$\bar{G}_\alpha = \bar{R}^*_{,\alpha} = \bar{g}_\alpha + \bar{u}_{,\alpha} + \theta^3 \bar{\lambda}_{,\alpha} \tag{19}$$

$$\bar{G}_3 = \bar{R}^*_{,3} = \hat{a}_3 + \bar{\lambda} \tag{20}$$

The metric tensor of the spatial coordinates of the deformed shell are given by

$$G_{\alpha\beta} = \bar{G}_\alpha \cdot \bar{G}_\beta \qquad G_{\alpha 3} = \bar{G}_\alpha \cdot \bar{G}_3 \tag{21}$$

Substituting for $\bar{G}_\alpha$ from Eq.(19), and carrying out the dot multiplication where the nonlinear displacement terms are neglected, we obtain

$$G_{\alpha\beta} = g_{\alpha\beta} + 2\gamma_{\alpha\beta} + 2\theta^3 \chi_{\alpha\beta} - (\theta_3)^2 (b_\alpha^\gamma \bar{a}_\gamma \cdot \bar{\lambda}_\beta + b_\beta^\gamma \bar{a}_\gamma \cdot \bar{\lambda}_{,\alpha}) \tag{22}$$

where

$$\gamma_{\alpha\beta} = \tfrac{1}{2} (\bar{a}_\alpha \cdot \bar{u}_{,\beta} + \bar{a}_\beta \cdot \bar{u}_{,\alpha}) \tag{23a}$$

$$\chi_{\alpha\beta} = \tfrac{1}{2} (\bar{a}_\alpha \cdot \bar{\lambda}_\beta + \bar{a}_\beta \cdot \bar{\lambda}_{,\alpha} - b_\alpha^\gamma \bar{a}_\gamma \cdot \bar{u}_{,\beta} - b_\beta^\gamma \bar{a}_\gamma \cdot \bar{u}_{,\alpha}) \tag{23b}$$

Similarly, substituting for $\bar{G}_\alpha$ and $\bar{G}_3$ from Eqs.(19)-(20), and recalling that $\bar{a}_\alpha$ and $\hat{a}_3$ are orthogonal, the components $G_{\alpha 3}$ in Eq.(21) are obtained as

$$G_{\alpha 3} = \bar{a}_\alpha \cdot \bar{\lambda} + \hat{a}_3 \cdot \bar{u}_{,\alpha} \tag{24}$$

The strain tensor is defined as

$$\bar{\gamma}_{ij} = \tfrac{1}{2} (G_{ij} - g_{ij}) \tag{25}$$

Substituting Eq.(12), Eq.(22) and Eq.(24) into Eq.(25), and neglecting the quadratic terms in θ^3 in view of the thin shell assumption, the strain tensor components are obtained as

$$\bar{\gamma}_{\alpha\beta} = \gamma_{\alpha\beta} + \theta^3 \chi_{\alpha\beta} \tag{26}$$

$$\bar{\gamma}_{\alpha 3} = \tfrac{1}{2} (\bar{a}_\alpha \cdot \bar{\lambda} + \hat{a}_3 \cdot \bar{u}_{,\alpha}) \tag{27}$$

The $\gamma_{\alpha\beta}$ is the middle surface strain component, and $\chi_{\alpha\beta}$ is the bending strain component linearly varying over the shell thickness. $\bar{\gamma}_{\alpha 3}$ is the transverse shear strain component. It may be observed that the components of the strain tensor throughout the shell are determined by the deformation of the middle surface, and are expressed in terms of the displacement vector $\bar{u}$, and the rotation vector $\bar{\Phi}$

In the next section, the strain tensor will be expressed in terms of cartesian components of the displacment and rotation vectors.

Strain Tensor in Cartesian Coordinates

The position vector to the middle surface, $\bar{R}_o(\theta^1,\theta^2)$, according to Eq.(1) is

$$\bar{R}_o(\theta^1,\theta^2) = x^1\hat{e}_1 + x^2\hat{e}_2 + x^3\hat{e}_3 = x^i\hat{e}_i \tag{28}$$

The tangent base vectors at the middle surface are

$$\bar{a}_\alpha = \bar{R}_{o,\alpha} = x^i{}_{,\alpha}\hat{e}_i \tag{29}$$

the unit normal vector to the middle surface is

$$\hat{a}_3 = n^i\hat{e}_i = \bar{a}_1 \times \bar{a}_2 / |\bar{a}_1 \times \bar{a}_2| \tag{30}$$

It can be shown that

$$|\bar{a}_1 \times \bar{a}_2| = \sqrt{a} \tag{31}$$

where a is the determinant of the metric tensor defined in Eq.(8). With the aid of Eq.(29) and Eq.(31), Eq.(30) becomes

$$\hat{a}_3 = n^i\hat{e}_i = \frac{1}{\sqrt{a}} e_{ijk}\, x^i{}_{,1}\, x^j{}_{,2}\, x^k{}_{,3} \tag{32}$$

where e_{ijk} is the permutation symbol.

The displacemnet vector and the rotation vector are expressed in terms of their cartesian components as

$$\bar{u} = v_1\hat{e}_1 + v_2\hat{e}_2 + v_3\hat{e}_3 \tag{33}$$

$$\bar{\Phi} = \beta_1\hat{e}_1 + \beta_2\hat{e}_2 + \beta_3\hat{e}_3 \tag{34}$$

With the help of Eq.(29), and Eq.(32)-(34), the strain tensor components in Eqs.(23)-(24) are expressed in terms of the cartesian components of the vectors $\bar{u}$ and $\bar{\Phi}$. The final equations using matrix notation, where the curvilinear coorindates θ^1 and θ^2 are denoted by α and β respectively, are as found below:

$$\{\gamma\} = [L_1]\{V\} \tag{35}$$

$$\{\chi\} = [L_2]\{V\} + [L_3]\{\beta\} \tag{36}$$

where

$$\{\gamma\} = \lfloor \gamma_{11}, \gamma_{22}, \gamma_{12} \rfloor^T \tag{37}$$

$$\{\chi\} = \lfloor \chi_{11}, \chi_{22}, \chi_{12} \rfloor^T \tag{38}$$

$$\{V\} = \left\lfloor \frac{\partial v_1}{\partial \alpha}, \frac{\partial v_2}{\partial \alpha}, \frac{\partial v_3}{\partial \alpha}, \frac{\partial v_1}{\partial \beta}, \frac{\partial v_2}{\partial \beta}, \frac{\partial v_3}{\partial \beta} \right\rfloor^T \tag{39}$$

$$\{\beta\} = \left\lfloor \beta_1, \beta_2, \beta_3, \frac{\partial \beta_1}{\partial \alpha}, \frac{\partial \beta_2}{\partial \alpha}, \frac{\partial \beta_3}{\partial \alpha}, \frac{\partial \beta_1}{\partial \beta}, \frac{\partial \beta_2}{\partial \beta}, \frac{\partial \beta_3}{\partial \beta} \right\rfloor^T \tag{40}$$

$$\underset{3\times 6}{[L_1]} = \begin{bmatrix} \partial x_1/\partial\alpha, & \partial x_2/\partial\alpha, & \partial x_3/\partial\alpha, & 0, & 0, & 0 \\ 0, & 0, & 0, & \partial x_1/\partial\beta, & \partial x_2/\partial\beta, & \partial x_3/\partial\beta \\ \frac{1}{2}\partial x_1/\partial\beta, & \frac{1}{2}\partial x_2/\partial\beta, & \frac{1}{2}\partial x_3/\partial\beta, & \frac{1}{2}\partial x_1/\partial\alpha, & \frac{1}{2}\partial x_2/\partial\alpha, & \frac{1}{2}\partial x_3/\partial\alpha \end{bmatrix} \tag{40}$$

$$\underset{3\times 6}{[L_2]} = \begin{bmatrix} -c_3, & -c_1, & -c_2, & 0, & 0, & 0 \\ 0, & 0, & 0, & -d_3, & -d_1, & -d_2 \\ -\frac{1}{2}d_3, & -\frac{1}{2}d_1, & -\frac{1}{2}d_2, & -\frac{1}{2}c_3, & -\frac{1}{2}c_1, & -\frac{1}{2}c_2 \end{bmatrix} \tag{41}$$

$$
[L_3]_{3\times 9} = \left[\begin{array}{c:c:c:c}
-\left(c_1\frac{\partial x_3}{\partial\alpha} - c_2\frac{\partial x_2}{\partial\alpha}\right) & -\left(c_2\frac{\partial x_1}{\partial\alpha} - c_3\frac{\partial x_3}{\partial\alpha}\right) & -\left(c_3\frac{\partial x_2}{\partial\alpha} - c_1\frac{\partial x_1}{\partial\alpha}\right) & a_1, a_2, a_3, 0, 0, 0 \\
\hdashline
-\left(d_1\frac{\partial x_3}{\partial\beta} - d_2\frac{\partial x_2}{\partial\beta}\right) & -\left(d_2\frac{\partial x_1}{\partial\beta} - d_3\frac{\partial x_3}{\partial\beta}\right) & -\left(d_3\frac{\partial x_2}{\partial\beta} - d_1\frac{\partial x_1}{\partial\beta}\right) & 0, 0, 0, b_1, b_2, b_3 \\
\hdashline
\begin{array}{l} -\frac{1}{2}\left(c_1\frac{\partial x_3}{\partial\beta} - c_2\frac{\partial x_2}{\partial\beta}\right. \\ \left. + d_1\frac{\partial x_3}{\partial\alpha} - d_2\frac{\partial x_2}{\partial\alpha}\right) \end{array} & \begin{array}{l} -\frac{1}{2}\left(c_2\frac{\partial x_1}{\partial\beta} - c_3\frac{\partial x_3}{\partial\beta}\right. \\ \left. + d_2\frac{\partial x_1}{\partial\alpha} - d_3\frac{\partial x_3}{\partial\alpha}\right) \end{array} & \begin{array}{l} -\frac{1}{2}\left(c_3\frac{\partial x_2}{\partial\beta} - c_1\frac{\partial x_1}{\partial\beta}\right. \\ \left. + d_3\frac{\partial x_2}{\partial\alpha} - d_1\frac{\partial x_1}{\partial\alpha}\right) \end{array} & \frac{b_1}{2}, \frac{b_2}{2}, \frac{b_3}{2}, \frac{a_1}{2}, \frac{a_2}{2}, \frac{a_3}{2}
\end{array}\right] \quad (4
$$

where

$$
a_1 = n_2\frac{\partial x_3}{\partial\alpha} - n_3\frac{\partial x_2}{\partial\alpha}, \quad a_2 = n_3\frac{\partial x_1}{\partial\alpha} - n_1\frac{\partial x_3}{\partial\alpha}, \quad a_3 = n_1\frac{\partial x_2}{\partial\alpha} - n_2\frac{\partial x_1}{\partial\alpha} \quad (44)
$$

$$
b_1 = n_2\frac{\partial x_3}{\partial\beta} - n_3\frac{\partial x_2}{\partial\beta}, \quad b_2 = n_3\frac{\partial x_1}{\partial\beta} - n_1\frac{\partial x_3}{\partial\beta}, \quad b_3 = n_1\frac{\partial x_2}{\partial\beta} - n_2\frac{\partial x_1}{\partial\beta} \quad (45)
$$

$$
c_1 = b_1^1\frac{\partial x_2}{\partial\alpha} + b_1^2\frac{\partial x_2}{\partial\beta}, \quad c_2 = b_1^1\frac{\partial x_3}{\partial\alpha} + b_1^2\frac{\partial x_3}{\partial\beta}, \quad c_3 = b_1^1\frac{\partial x_1}{\partial\alpha} + b_1^2\frac{\partial x_1}{\partial\beta} \quad (46)
$$

$$
d_1 = b_2^1\frac{\partial x_2}{\partial\alpha} + b_2^2\frac{\partial x_2}{\partial\beta}, \quad d_2 = b_2^1\frac{\partial x_3}{\partial\alpha} + b_2^2\frac{\partial x_3}{\partial\beta}, \quad d_3 = b_2^1\frac{\partial x_1}{\partial\alpha} + b_2^2\frac{\partial x_1}{\partial\beta} \quad (47)
$$

Similarly, the components of the transverse shear strain tensor in Eq.(27) are also expressed in terms of cartesian components:

$$2\gamma_{\lambda 3} = (\beta_2 n_3 - \beta_3 n_2) x_{1,\lambda} + (\beta_3 n_1 - \beta_1 n_3) x_{2,\lambda} + (\beta_1 n_2 - \beta_2 n_1) x_{3,\lambda} + n_1 v_{1,\lambda} + n_2 v_{2,\lambda} + n_3 v_{3,\lambda} \quad (48)$$

where $\lambda = 1,2$ corresponds to the coordinate directions α and β respectively.

Strain energy density

The strain energy density per unit volume in a three dimensional elastic body is of the form

$$u = \frac{1}{2} \tau^{kl} \bar{\gamma}_{kl} \quad (49a)$$

where τ^{kl} are the contravariant components of the stress tensor. The three dimensional stress-strain relations for linear elastic behaviour are of the form

$$\tau^{ij} = E^{ijkl} \bar{\gamma}_{kl} \quad (49b)$$

where the E^{ijkl} (i,j,k,l: 1,2,3) are the components of the constitutive tensor. For an isotropic material the constitutive tensor can be expressed in terms of the two elastic constants of the material [23] in the form

$$E^{ijkl} = \frac{E}{2(1+\nu)} \left[g^{ik} g^{jl} + g^{il} g^{jk} + \frac{2\nu}{1-\nu} g^{ij} g^{kl} \right] \quad (50)$$

where E is the Young's modulus and ν is the Poisson's ratio.

In the case of thin shell under plane stress assumption, and when the strain distribution is given by Eqns.(26)-(27), the strain energy density per unit area of the middle surface, u_s, is obtained from Eq.(50) as [23]

$$u_s = \frac{1}{2}\Big(h C^{\alpha\beta\gamma\eta}\gamma_{\alpha\beta}\gamma_{\gamma\eta} + \frac{h^3}{12}C^{\alpha\beta\gamma\eta}\chi_{\alpha\beta}\chi_{\gamma\eta}$$

$$+ 4hE^{\alpha 3\beta 3}\gamma_{\alpha 3}\gamma_{\beta 3}\Big) \qquad (51)$$

where

$$C^{\alpha\beta\gamma\eta} = \frac{E}{2(1+\nu)}\left[a^{\alpha\gamma}a^{\beta\eta} + a^{\alpha\eta}a^{\beta\eta} + \frac{2\nu}{1-\nu}a^{\alpha\beta}a^{\gamma\eta}\right] \qquad (52)$$

and h is the shell thickness. It is observed that the strain energy density in the thin shell has been expressed as the sum of that due to stretching, bending and transverse shear. In case of thin shells, the contribution of the transverse shear strain energy to the total energy is small, and will be completely neglected from further considerations. When the transverse shear energy is neglected, the strain energy density can be expressed in matrix notation as

$$u_s = \frac{1}{2}\lfloor\gamma\rfloor[D]\{\gamma\} + \frac{1}{2}\lfloor\chi\rfloor[E]\{\chi\} \qquad (53)$$

where

$$[E] = \frac{h^2}{12}[D] \qquad (54)$$

$$[D] = \left[\begin{array}{c|c|c} (a^{11})^2 & (1-\nu)(a^{12})^2 + \nu a^{11}a^{22} & 2a^{11}a^{12} \\ \hline \text{SYM.} & (a^{22})^2 & 2a^{22}a^{12} \\ \hline & & 2(1-\nu)a^{11}a^{22} + 2(1+\nu)(a^{12})^2 \end{array}\right]$$

In the next section the finite element discretization of the strain energy is presented.

FINITE ELEMENT DISCRETIZATION

Coordinate System

Figure 3 shows the element geometry and the various coordinate systems employed where the curvilinear coordinates are denoted by (α, β). The element is defined in the (α,β)-parametric plane as shown in Figure 3b, where the nodes are specified by their (α, β) coordinates and the element sides are specified as straight lines. This plane triangle is mapped onto the curvilinear element in the three dimensional space by the parametric equations of the shell middle surface as shown in Figure 3a. The shell middle surface is defined by the components of the position vection $\bar{R}_0(\alpha, \beta)$ in a global cartesian coordinate system as given by Eq.(1). Figure 4c shows the (ξ, η) natural coordinate system where the triangle in the parametric plane is mapped onto the unit right-angled triangle. The mapping is defined by the transformation

$$\alpha = \alpha_1 + (\alpha_2 - \alpha_1)\xi + (\alpha_3 - \alpha_1)\eta \tag{56}$$

$$\beta = \beta_1 + (\beta_2 - \beta_1)\xi + (\beta_3 - \beta_1)\eta \tag{57}$$

where ξ and η vary from 0 to 1. The mapping is unique and one-to-one provided the Jacobian of the transformation

$$J = (\alpha_2 - \alpha_1)(\beta_3 - \beta_1) - (\alpha_3 - \alpha_1)(\beta_2 - \beta_1) \tag{58}$$

does not vanish

Interpolation of Displacement and Rotation components

The Cartesian components of the displacement vector, v_i (i=1,2,3), are interpolated by complete (ten-term) cubic polynomial in the $(\xi-\eta)$ natural coordinates. The interpolation is represented in the shape function form as

$$V_i = \lfloor N_T \rfloor \{V_i\} \qquad (i = 1,2,3) \tag{59}$$

where

$$\{V_i\} = \lfloor (V_i)_1, \left(\frac{\partial V_i}{\partial \alpha}\right)_1, \left(\frac{\partial V_i}{\partial \beta}\right)_1, ----, \left(\frac{\partial V_i}{\partial \beta}\right)_3, (V_i)_G \rfloor^T \tag{60}$$

The suffix following the parantheses indicates the node number or the centroid. The shape functions $\lfloor N_T \rfloor$ are detailed in Reference[2].

The Cartesian components of the rotation vector, β_i(i=1,2,3), are interpolated by complete (six-term) quadratic polynomials in $(\xi-\eta)$ coordinates from their nodal values at the three corner nodes and three mid-side nodes. Thus

$$\beta_i = \lfloor N_R \rfloor \{\beta_i\} \qquad (i = 1,2,3) \tag{61}$$

where

$$\underset{6\times 1}{\{\beta_i\}} = \lfloor (\beta_i)_1, (\beta_i)_2, (\beta_i)_3, ----, (\beta_i)_6 \rfloor^T \tag{62}$$

The shape functions $\lfloor N_R \rfloor$ are detailed in Reference [3].

The above representations for the displacement and rotation components result in a total of 48 degrees of freedom (DOF). Subsequently these are reduced to 27 DOF by imposition of various constraints and static condensation of the centriodal. freedoms to be discussed later.

Isoparametric Representation of the Element Geometry

The geometry of the middle surface is described by the position vector and its $(\alpha-\beta)$ derivatives up to second order. The nodal values of these geometric quantities are obtained from the parametric equations of the shell middle surface. The geometric quantities within the element are, however, obtained by interpolating the position vector within the element using the same shape functions as those used for the displacements.

Thus the components of the position vector at any point (ξ,η) within the element are obtained as

$$x_i(\xi,\eta) = \lfloor N_T \rfloor \{x_i\} \qquad (i=1,2,3) \tag{63}$$

where the vector $\{x_i\}$ is defined similar to Eq.(60). It can be shown that [5] this isoparametric representation of the element geometry leads to an exact representation of the rigid body modes of the shell. It may be noted that the cubic representation of the shell surface is C^1- continuous at the element nodes, but is only C^0- continuous across the inter element boundaries. It has been shown by Ciarlet[24] that this is sufficient to provide the "geometric conformity". Thus the element is conforming for both the displacemnets as well as geometry.

Constraint Conditions

Although the use of shear deformation theory has led to a conforming element with the use of simple polynomial shape functions, this also renders the element unduly stiff and resuls in a slow convergence rate [21]. It is desirable to alleviate the effects of the transverse shear deformation to achieve a faster convergence to the thin-shell solution.

The first step towards the above was taken in neglecting the transverse shear energy. To reduce the effects further, constraints analogous to Kirchhoff hypothesis are imposed at a discrete number of points on the element boundary which will be referred to as discrete Kirchhoff constraints (DKC)

It is also observed that the independent assumption for the displacement and rotation components leaves the rotation of the shell about the normal doubly defined. One value is defined in terms of the displacement gradients, and a second value in terms of independent rotation components. Six constraints representing the equality of these two values are imposed, one at each of the corner and mid-side nodes, which will be referred to as surface normal rotation constraints (SNRC). Finally, the rotation degrees of freedom at the mid-side nodes are eliminated by imposing constraints of linear variation of the normal rotation along the element sides (LVNRC). A brief derivation of these constraints follows.

The six DKC at the corner nodes are given by the conditions

$$(\gamma_{\lambda 3})_j = 0 \qquad j = 1,2,3;\ \lambda = 1,2 \qquad (64)$$

where the suffix j stands for the node number, and λ = 1,2 corresponds to the coordinate directions α and β respectively. The expression for $\gamma_{\lambda 3}$ is given by Eq.(27), which in the present notation becomes

$$2\gamma_{\lambda 3} = (\beta_2 n_3 - \beta_3 n_2)\chi_{1,\lambda} + (\beta_3 n_1 - \beta_1 n_3)\chi_{2,\lambda} + (\beta_1 n_2 - \beta_2 n_1)\chi_{3,\lambda} + n_1 v_{1,\lambda} + n_2 v_{2,\lambda} + n_3 v_{3,\lambda} \quad (\lambda = 1,2) \tag{65}$$

The three DKC at the mid-side nodes are given by the conditions

$$(\gamma_{s3})_k = 0 \qquad k = 4,5,6 \tag{66}$$

where γ_{s3} is the transverse shear strain between the normal direction and the direction, s, tangential to the curvilinear side; k is the mid-side node. The γ_{s3} component is obtained in terms of the transverse shear components along the α and β directions following the second-order tensor transformation law. Thus we obtain

$$\gamma_{s3} = \frac{\partial \theta^\lambda}{\partial s}\gamma_{\lambda 3} \qquad Sum\ on\ \lambda\ ,\ (\lambda = 1,2) \tag{67}$$

where θ^1 and θ^2 correspond to α and β directions, and s is a parameter varying along the element side. The coefficients of transformation in Eq.(67) can be obtained by observing that the sides of the unit triangle in the (ξ,η) coordinate plane are mapped onto the corresponding curvilinear sides of the element in the Eucledean space as shown in Figure 3; and thus we can consider $(\xi - \eta)$ coordinates as an alternative set of parameters. In view of Eqns.(56)-(57) we thus obtain

$$\gamma_{s3} = \alpha_{ji}\gamma_{13} + \beta_{ji}\gamma_{23} \tag{68}$$

where $\alpha_{ji} = (\alpha_j - \alpha_i)$ etc., and i and j are the corner nodes on the element side.

The surface normal rotation constraint (SNRC) is specified by the condition of equality of the two values of Ω, the shell rotation about the normal, as discussed earlier. Thus,

$$(\Omega^{(1)})_i = (\Omega^{(2)})_i \qquad (i = 1, 2, \ldots, 6) \tag{69}$$

where i stands for the node number. The $\Omega^{(1)}$ is given in terms of rotations as

$$\Omega^{(1)} = n_1 \beta_1 + n_2 \beta_2 + n_3 \beta_3 \tag{70}$$

The $\Omega^{(2)}$, defined in terms of displacement gradients, can be shown to be [25]

$$\Omega^{(2)} = \frac{1}{2\sqrt{a}} \left[(x_{1,\beta} V_{1,\alpha} - x_{1,\alpha} V_{1,\beta}) + (x_{2,\beta} V_{2,\alpha} - x_{2,\alpha} V_{1,\beta}) \right.$$

$$\left. + (x_{3,\beta} V_{3,\alpha} - x_{3,\alpha} V_{3,\beta}) \right] \tag{71}$$

Finally the constraints of linear variation of the normal rotation along the element side are given by the equation

$$(\beta_s)_k = \frac{1}{2} [(\beta_s)_i + (\beta)_s)_j] \qquad (k = 4, 5, 6) \tag{72}$$

where β_s is the rotation vector component along the tangent to the element side, and k is the mid-side node on the side joining the corner nodes i,j.

Using the above set of 18 constraints the rotation degrees of freedom at any of the nodes can be expressed in terms of the displacement degrees of freedom. Thus we can eliminate the rotation degrees of freedom completely leading to a finite element with 30 DOF consisting of the displacements and their derivative values at the corner nodes and the centriodal displacements.

Calculation of Element Matrices

The element stiffness matrix and the load vector are obtained by use of the principle of minimum potential energy. The total potential energy in an element is

$$\pi_p^{(e)} = U^{(e)} + H^{(e)} \tag{73}$$

where $U^{(e)}$ is the element strain energy, and $H^{(e)}$ is the potential energy of the extenral loads. If the components of the external distributed loading in the cartesian directions are denoted as P_i (i=1,2,3), then

$$H^{(e)} = -\int_{Area} P_i v_i \sqrt{a}\, d\alpha\, d\beta \qquad (i = 1,2,3) \tag{74}$$

The element strain energy is given by

$$U^{(e)} = \int_{Area} u_s \sqrt{a}\, d\alpha\, d\beta \tag{75}$$

where u_s is the strain energy density given by Equation (53). Th minimization of the total potential energy of the element with respect to the nodal degrees of freedom leads to the element stiffness matrix and the consistent load vector. The i-j th element of the stiffness matrix [k] is given by

$$k_{ij} = \frac{\partial^2 U^{(e)}}{\partial v_i \partial v_j} \qquad (i, j = 1\text{-}30) \tag{76}$$

Similarly, the i-th component of the load vector due to the j-th component of the distributed load is given by

$$F_i^{(\gamma)} = \frac{\partial H^{(e)}}{\partial V_i} \quad (i = 1\text{-}30) \tag{77}$$

The computational procedure for the calculation of k_{ij} and $F_i^{(\gamma)}$, where the constraint conditions are numerically incorporated without deriving the discrete Kirchhoff shape functions explicitly, follows along the similar lines as detailed in Reference [2]. The explicit derivation of the latter shape functions is extremely tedius, since all the displacement components are coupled in the constraint conditions.

As a last step in the element formulation, in order to apply the symmetric and support conditions easily, the element matrices are transformed to a local orthoganal curvilinear coordinate system. The unit vectors of the latter coordinate system are defined by the orthogonal vector triad $\hat{t}_1, \hat{t}_2 = \hat{n} \times \hat{t}_1$ and $\hat{n}$, where $\hat{t}_1$ is the unit vector along $\bar{a}_1$ and $\hat{n}$ is the surface unit normal vector. The transformation follows the standard procedure, and the details may be found in Reference [25]. Finally, the centroidal freedoms are removed by static condensation leading to element matrices of size 27 X 27, with tangential and normal displacements and their first order derivatives with respect to (α, β) coordinates as the final nodal freedoms.

The triangular thin shell finite element developed here has been named "KSHARA", meaning "finite" in one of its connotations.

NUMERICAL RESULTS

Results from the present element for plate problems would be identical to those presented in the earlier papers of the authors [2,26]. The results for cylindrical shell problems where the rigid-body type motion is not predominant were also reported in Reference [2], and the present results for these problems are not significantly different. However, a few additional cylindrical shell problems and those of other regular geometries are considerd here.

Infinite Fixd-Free Quarter Cylinder

A quarter of an infinitely long cylinder with one end fixed and other end free subjected to a uniform pressure load, as shown in Figure 4, is considered. Due to symmetry a strip of the cylinder was discretized with element orientations as shown in the same figure. The convergence of normal displacement of the free edge for various values of the thickness ratio along with an analytical solution reported in Reference [12] is presented in Table 1. The results indicate excellent agreement between the two for all the thickness ratios with the maximum error less than one percent.

Pinched Cylinder With Supported Edges

A thin pinched cylinder with freely supported (diaphragm) ends acted upon by two pinching loads at the centre of the cylinder is considered. The geometric details and a 5 X 5 nonuniform grid in the cylinder octant, where the ratios of the successive element-side lengths to that of the smallest are 2,3,4 and 5 respectively, are shown in Figure 5. The problem is considered to be a critical test case due to the combined effects of the concentrated loads and the support conditions.

Table 2 shows the comparison of the displacements at various points on the shell with the alternative finite element and analytical solutions. The finite element solution is based on the transformed shallow shell element of Lindberg, Olson and Cowper[27], and the analytical solution is based on a double Fourier series solution, also reported in Reference [27]. It is seen that the normal deflection under the pinching load, which is proportional to the strain energy of the shell, is predicted within one percent of the comparitive finite element solution, and two percent of the analytical solution. The normal displacement of the point B seems to be most difficult to predict, as also shown by the alternative finite element solution. The axial displacement of the point D on the diaphragm edge is within two percent of the analytical value. Figure 6 shows the distribution of the membrane stress and bending moment resultants along the line BC of the pinched cylinder along with the analytical solution. A close agreement between the two is observed.

<u>Spherical shell under internal pressure</u>

A spherical shell under internal pressure is in a pure membrane state of stress where both the meridional and hoop stress components are given by PR/2. The present example is a test for the element to represent a constant membrane state of stress.

A spherical shell with the α-β curvilinear coordinate system, along with a nonuniform finite element mesh in a portion of the shell between two meridians, as shown in Figure 7, is considered. The displacement and stress resultants at the pole and the equator are compared against the exact solution in Table 3. A fast convergence towards exact solution is observed for both the displacements and stress resultants. The comparison of stress resultants is better than that of the displacements. The small difference in the displacements may be due to the cubic approximation of the spherical shell surface, and an improvement in accuracy can, however, be achieved by increasing the number of elements in the meridional direction.

Torus under internal pressure

The analysis of a toroidal shell subjected to internal pressure is considered next. In a toroidal shell both the regions of positive and negative Gaussian curvature are present. The geometry of a torus along with the parametric equations of the shell surface are shown in Figure 8. The parameters of surface representation are chosen as the angles (α, β) whose coordinate lines coincide with the lines of curvature.

In view of the horizontal plane of symmetry and the axisymmetric loading a sector of the shell with an included angle of 8 degrees is discretized with 15 meridional divisions with orientations as shown in Figure 8. The mesh is non-uniform, being crowded toward the point $\alpha = 90°$, but maintaining symmetry on either side of it.

The displacement and stress resultants at various points in the shell are compared with the numerical solution of Kalnins [28] for two values of the h/b ratio (0.05 and 0.005) as displayed in Table 4. Kalnins' numerical solution is a combination of the direct-integration approach and a finite difference scheme, and is referred to as multi-segment integration.

A study of the results in Table 4 shows that very good agreement between the present finite element solution and the comparative solution has been achieved for both the displacement as well as stress resultants. In Figure 9 the normal displacement distribution along the meridian is compared with kalnins' solution. A comparison of meridional stress distributions is presented in Figure 10. There is a very close agreement of both the solutions for the membrane and bending components. A sharp rise in the bending stress near the region of $\alpha = 90$ is in agreement with the earlier observations [28] that when a middle surface touches a plane-closed curve, in the vicinity of this point high bending stresses should be expected.

A Hemispherical shell under concentrated loads at the open edge

A patch test problem with an engineering appeal proposed by Morley and Morris [22] is considered. This problem is directed at predominantly inextensional bending through the solution of a hemispherical shell subjected to concentrated loading actions as shown in Figure 11.

The finite element discretization of the symmetric one quarter of the shell shown in Figure 11 contains 51 elements with 35 nodal points resulting in 261 active degrees of freedom. The comparison of normal deflection of the point 2 ($\phi = \pi/2$, $\theta = 0$) against the alternative finite element and numerical solution reported by Morley and Morris [22] is displayed in Table 5.

Two numerical solutions using the Rayleigh - Ritz method are presented in Reference [22]. The first solution is a single series solution which considers only the inextensional mode of behaviour. Such a solution is obtained using the general inextensional solution in conjunction with the principle of minimum potential energy. This solution is a lower bound for the displacement and does not account for the membrane and edge effects. The second solution is obtained by a similar procedure using double trigonometric series which attempts to include the membrane and edge effects. It is observed from Table 5 that the KSHARA element recovers the theoretical value exactly. All the alternative finite element solutions recover the theoretical value within at least 8%

accuracy.

Various other patch test solutions for spherical shells derived in Reference [22] have been applied [25], the results of which will be reported in a separate publication. These patch test solutions form an indirect verification of the compliance of the conditions of conformity and convergence for this class of shells.

CONCLUSIONS

The objective of the research work presented here was to develop a thin shell finite element to model arbitrary thin shells which would be efficient and simple to use by the practicing engineer. The satisfaction of the mathematical requirements to ensure a sound theoretical basis was also, however,considered as equally important. To that end, the development of a deep shell finite element based on discrete Kirchhoff approach with an explicit representation of rigid body modes through an isoparametric representation of the shell surface was sought . The displacement and rotation components were interpolated by cubic polynomial shape functions using simple nodal connections. The final degress of freedom are the displacement components and their first order derivatives with reference to a local orthogonal curvilinear coordinate system, which enables easy application of the support conditions. The element performance was evaluated through a number of bench mark thin shell problems of various shapes under different support and loading conditions. The results of a "patch test" problem were also included demonstrating the satisfactory performance of the element under limiting states of behaviour.

It may be thus seen that the discrete kirchhoff theory approach in conjunction with an isoparametric representation of the shell geometry has resulted in a simple conforming thin shell element meeting a majority of the features sought in engineering applications. The element is efficient and gives results of engineering accuracy for a variety of shells under different support and loading conditions. The approximation of the shell geometry by cubic polynomials has been apparently satisfactory for a majority of practical shells.

A simple modification of the element wherein the mid-side nodes are retained would improve the convergence rate consequent of the resulting quadratic variation of the normal rotation along the element sides.

REFERENCES

1. Irons, B.M. and K.J Draper, " Inadequacy of Nodal conections in a Stiffness solution for plate Bending ", AIAA, J., Vol.3, pp.61, 1965.

2. Murthy, S.S. and R.H. Gallagher, "An Anisotropic cylindrical shell Element Based on Discrete kirchhoff Theory", Int.J.Num. Meth. Engng., Vol.19, No.12, pp.1805-18, 1983.

3. Batoz, J.L., K.J.Bathe and L.W. Ho, "A study of Three-node Triangular Plate Bending Elements",Int. J.Num. Meth. in Engng., Vol.15, pp.1771-1812, 1980.

4. Batoz, J.L. and G.Dhatt, "An Evaluation of Two simple and Effective Triangular and Quadrilaterl plate Bending Elements" in Proc.of New and Future Developments in Commercial Finite Element Mehtod, Los Angeles, California, pp.352-68,1981.

5. Dupuis, G., "Application of Ritz's Method to Thin Elastic Shell Analysis", Trans.ASME, J.Appl.Mech., Ser.E, vol.38, No.4, pp.987-96, 1971.

6. Clement, P. and J.Descloux, "On the Rigid Body Displacement Condition", Int J.Num.Meth.Engng., Vol.4, No.4, pp.583-86, 1972.

7. Cowper, G.R., "CURSHL: A High-Precision Finite Element for shells of Arbitrary Shape", Aeronautical Report - LR - 560, National Research Council of Canada, Ottawa, December 1971.

8. Thomas, G.R and R.H.Gallagher, "A Triangular Thin Shell Finite Element: Linear Analysis", NASA CR-2482, July 1975.

9. Morris, A.J., "A Summary of Appropriate Governing Equations and Functionals in the Finite Element Analysis of Thin Shells", in Finite Elements for Thin Shells and Curved Members (Eds. D.G.Ashwell and R.H.Gallagher), John Wiley, 1976, Chapter 2.

10. Argyris, J.H., and D.Scharpf, "The SHEBA Family of Shell Elements for the Matrix Displacement Method", Aeronautical J., Vol.72, pp.873-83, 1968.

11. Wu, S.-C. and J.F.Abel, "Representation and Diseretization of Arbitrary Surfaces for Finite Element Shell Analysis," Int.J.Num.Meth. Engng., Vol.14, pp.813-836, 1979.

12. Wu, S.- C., "An Integrated System for Finite Element Shell Analysis - Surface Representation and Curved Shell Element", Ph.D. Dissertation, Cornell University, Ithaca, N.Y., 1980.

13. Birkhoff, G., and Mansfield, L., "Compatible Triangular Finite Elements", J.Math.Anal.Appl., Vol.47, pp.531-53, 1974.

14. Irons, B.M., and A.Razzaque, "Shape Function Formulations for Elements other than Displacement Methods", in Proc.Int.Conf. on Variational Methods in Engng, Southampton, 1972.

15. Irons, B.M., and A.Razzaque, "Experience with Patch Test", in Mathematical Foundations of the Finite Element Methods, (Eds. A.R.Aziz), Academic Press, 1972.

16. Chang.S.-C., "An Integrated Finite Element Nonlinear shell Analysis System with Interactive Computer Graphics", Ph.D. Dissertation, Cornell University, Ithaca, N.Y., 1981.

17. Dhatt, G., "An Efficient Triangular Shell Element", AIAA J., Vol.8, No.11, pp.2100-2102, 1970

18. Batoz, J.L., and G.Dhatt, "Development of Two Simple Shell Elements", AIAA J., Vol.10, No.2, pp.237-38, 1972

19. Batoz,J.L., "Analyse non Lineaire Des Coques Minces Elastiques De Formes Arbitraries Par Elements Triangularies Coubes" (in French), D.Sc. dissertation, U.of Laval, Quebec, Canada, March 1977.

20. Wempner,G.A., J.T.Oden and D.A.Kross, "Finite Element Analysis of Thin Shells", Proce.ASCE, J.Engng.Mech.Division No.EM 6, pp. 1273-1294, 1968.

21. Batoz,J.L., A. Chattopadhay and G.S.Dhatt, "Finite Element Large Deflection Analysis of Shallow Shells", Int. J.Num.Meth Engng.,Vol.10, No.1, pp.39-58, 1976.

22. Morley, L.S.D and A.J.Morris, "Conflict Between Finite Elements and shell Theory", in Finite Element Methods in the Commercial Enviornment (Ed.John Robinson), Vol.2, Robinson and Associates, England, 1978.

23. Wempner,G.A., Mechanics of Solids With Application to Thin Bodies, McGraw Hill, N.Y., 1977.

24. Cierlet,P.G., Numerical Analysis of the Finite Element Method., Les Presses De L'Universite De Montréal, Canada, 1976, Section 16, pp.271-72.

25. Murthy,S.S., A Triangular Anisotropic Thin Shell Element Based on Discrete Kirchhoff Theroy, Ph.D. Dissertation, The University of Arizona, Tucson, Arizona, 1983.

26. Murthy,S.S., "Discrete Kirchhoff Theory plate Element and work Equivalent Load", Int.J.Num.Meth.Engng., Vol.19, pp 1732-37, 1983.

27. Lindberg,G.M., M.D.Olson and G.R.Cowper, "New Developments in the Finite Element Analysis of Shells", Reprint of article from DME/NAE Quarterly Bulletin, No.1969(4), NAE, National Research Council of Canada, 1970.

28. Kalnins,A., "Analysis of Shells of Revolution Subjected to Symmetrical and nonsymmetrical Loads", Trans. ASME, J.of Applied Mechanics Series E., Vol.86, pp.467-76, 1964.

Table 1. Convergence of normal displacement at the free edge of the fixed-free quarter cylinder under distributed edge moment.

	$wEh^3/(R^2M)$		
N[a]	h/R = 0.001	0.01	0.1
4	10.77	11.59	11.79
8	10.96	11.67	11.88
32	10.97	11.72	11.93
Analytical Solution[b]	10.92	10.92	10.92

[a] N = No. of circumferential divisions.

[b] Analytical solution is [12]: $wEh^3/(MR^2) = 12(1 - \nu^2)$.

Table 2 Comparison of displacements for the pinched cylinder with supported edges.

Grid size in quarter shell	$\frac{Ehw_C}{P}$	$\frac{Ehw_B}{P}$	$\frac{Ehu_D}{P}$
5X5	-157.3470	-7.8647	3.9804
8X8	-160.7760	-5.5209	4.0212
5X5 [27] non-uniform	-159.23	-4.63	3.954
Analytical [27]	-164.24	-0.47	4.114

Table 3 Comparison of displacements and stress resultants for spherical shell under internal pressure.

Mesh size (No. of Eqs.)	Normal displacement Ehw/pR^2		Stress resultants			
			At pole		At equator	
	At pole	At equator	$\frac{N}{pR}$	$\frac{N}{pR}$	$\frac{N}{pR}$	$\frac{N}{pR}$
2X4 (57)	0.4138	0.3470	0.5276	0.4860	0.5279	0.5194
2X10 (147)	0.35321	0.3457	0.5097	0.4964	0.5173	0.5139
2X15 (222)	0.35079	0.34506	0.5056	0.5005	0.51700	0.5135
Exact	0.3500	0.3500	0.5000	0.5000	0.5000	0.5000

Table 4 Comparison of displacements and stress resultants for torus under internal pressure.

Meridional angle degrees	(a) Comparison of normal displacement		(b) Comparison of meridional stresses			
	Normal displacement $\frac{w}{b}x10^3$		Meridional membrane stress $(\sigma_{1m}/E)x10^3$		Meridional bending stress $(\sigma_{1b}/E)x10^3$	
	$\frac{h}{b}=0.05$	$\frac{h}{b}=0.005$	$\frac{h}{b}=0.05$	$\frac{h}{b}=0.005$	$\frac{h}{b}=0.05$	$\frac{h}{b}=0.005$
0	0.1036 (0.103)[a]	0.10055 (0.1000)	3.982	3.996 (3.997)[a]	--	--
81	4.1991 (4.208)	5.060 (5.151)	1.8573	2.170 (2.104)	2.058 (2.053)	1.509 (1.520)
180	1.2574 (1.249)	1.3017 (1.298)	1.6106	1.607 (1.601)	--	--

[a]Values in the parentheses from Ref. [28].

Table 5 Comparison of normal displacement for the hemispherical shell under concentrated loads.

Element	Angle subtended in degrees	Normal displacement of point 2 WD/P_2R^2
SEMILOOF	18	0.179
SEMILOOF FACET	18	0.184
SHEBA 6	22.5	0.175
MSC/NASTRAN	9	0.188
BAE FACET	9	0.188
KSHARA	18	0.185
Theoretical		
Double trigonometric series solution	0.185	
Inextensional solution	0.173	

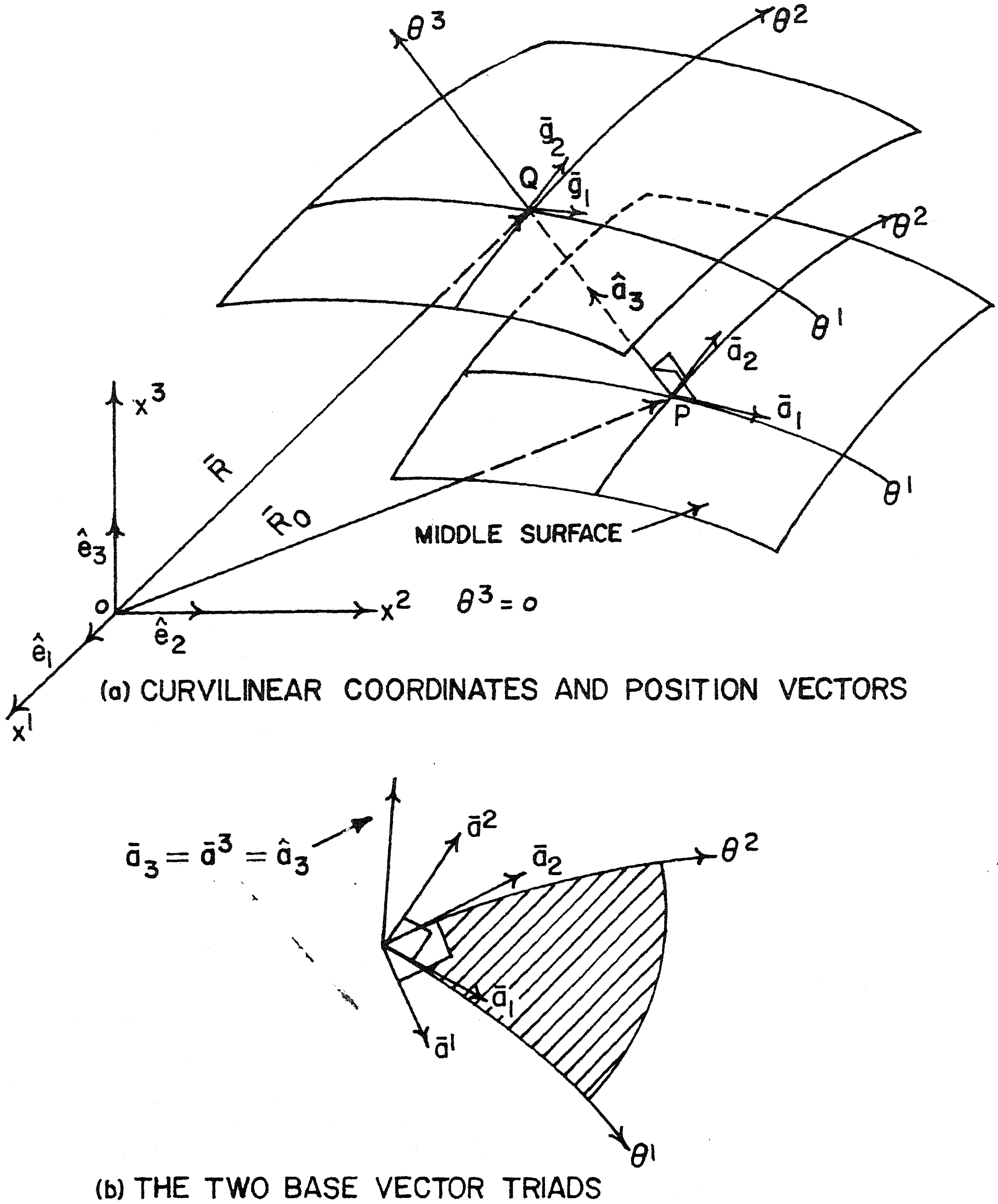

Figure 1 Curvilinear coordinates and base vectors.

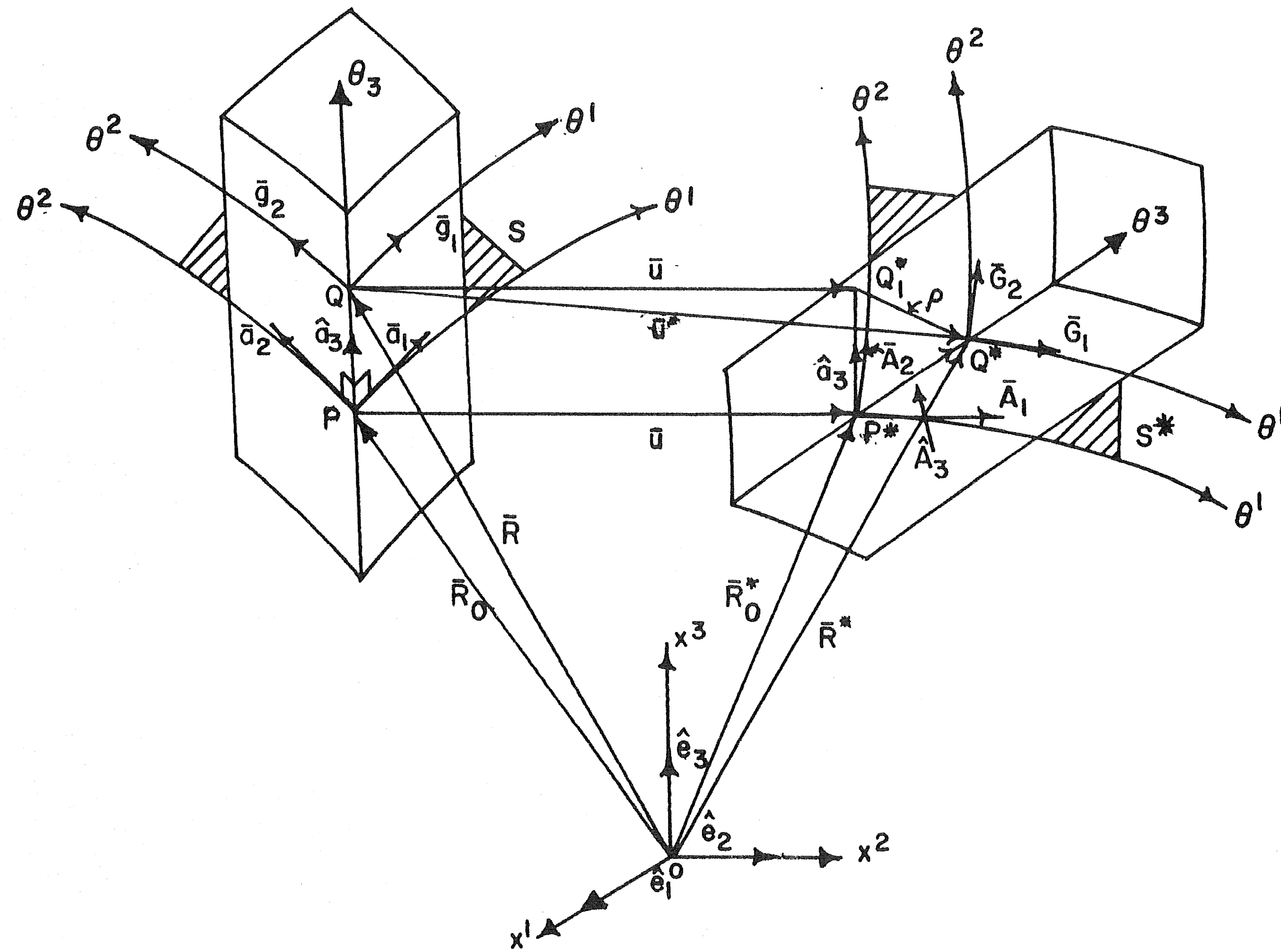

Figure 2 Motion of a shell element.

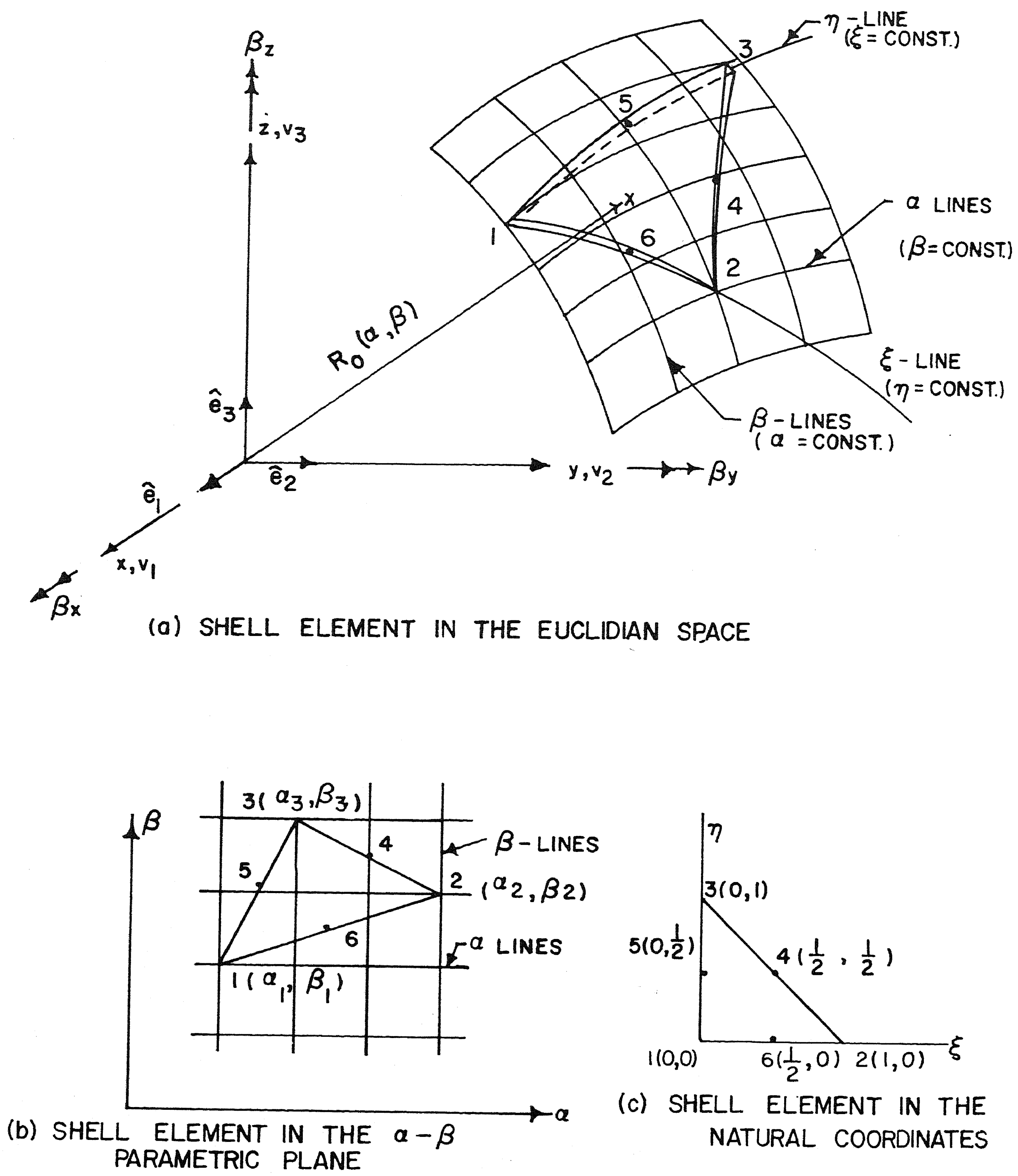

Figure 3 Coordinate systems.

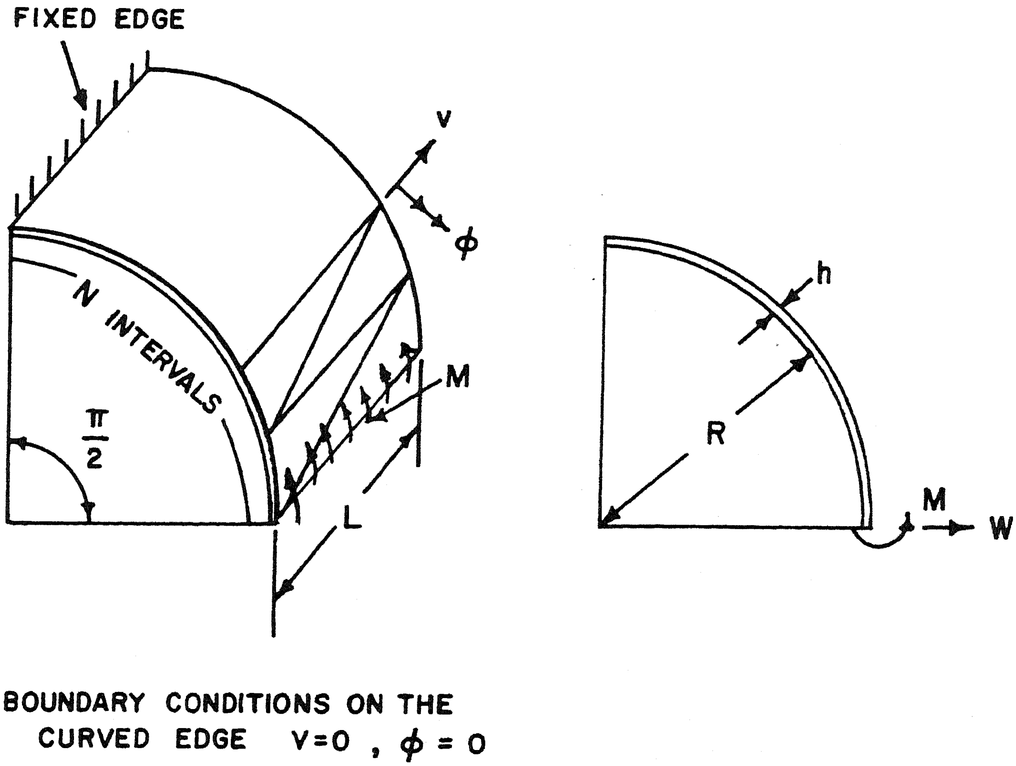

Figure 4 Fixed free quarter cylinder under uniform pressure.

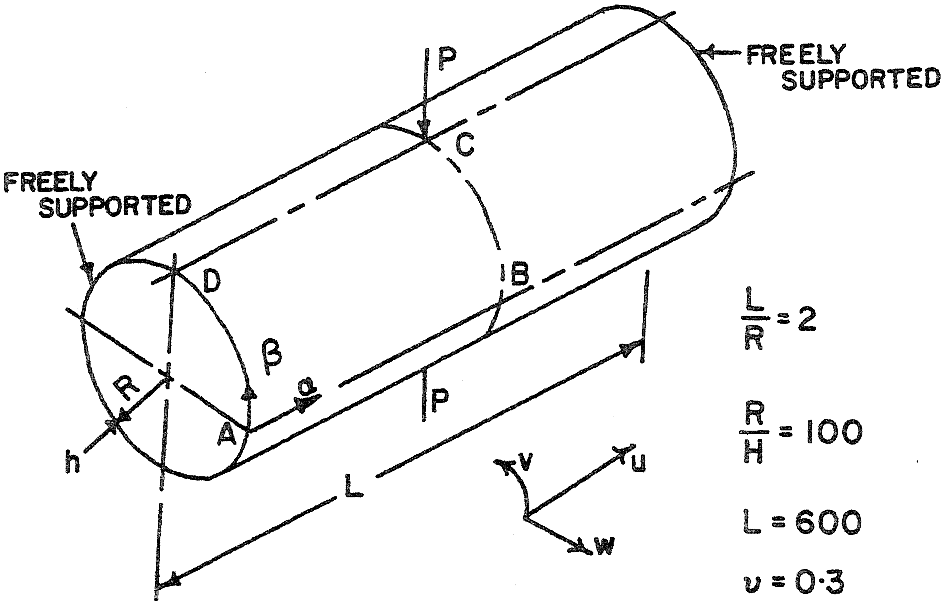

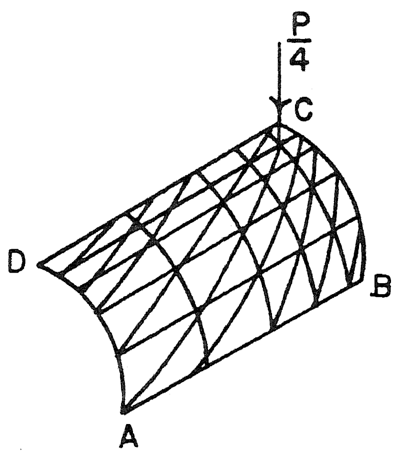

5X5 GRID IN THE QUARTER-CYLINDER

Figure 5 Pinched cylinder with supported edges.

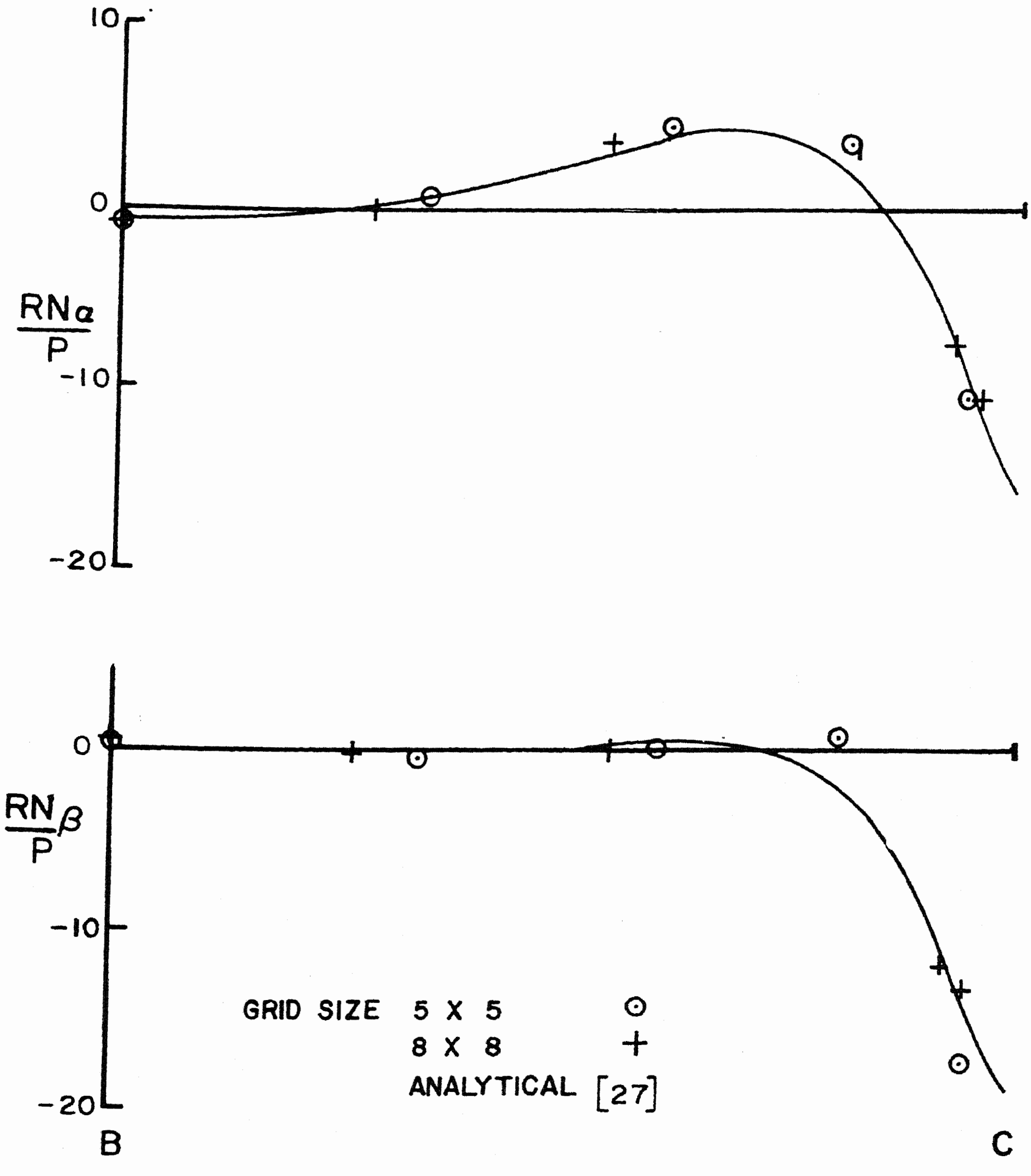

Figure 6 Membrance stress and bending moment distribution along the line BC for the pinched cylinder with supported edges.

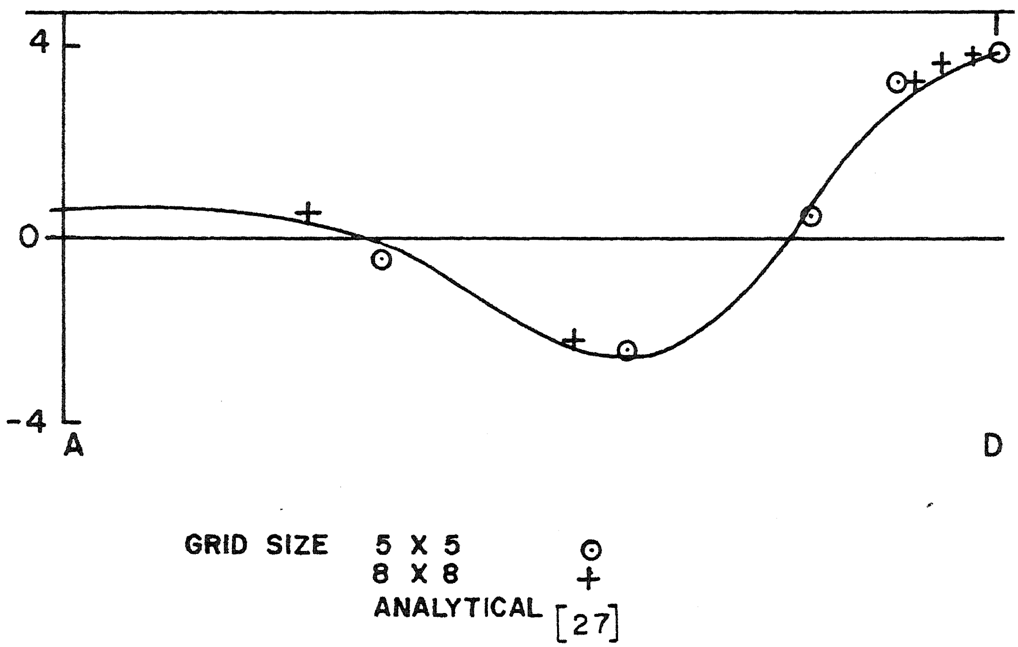

Fig.6: Continued.

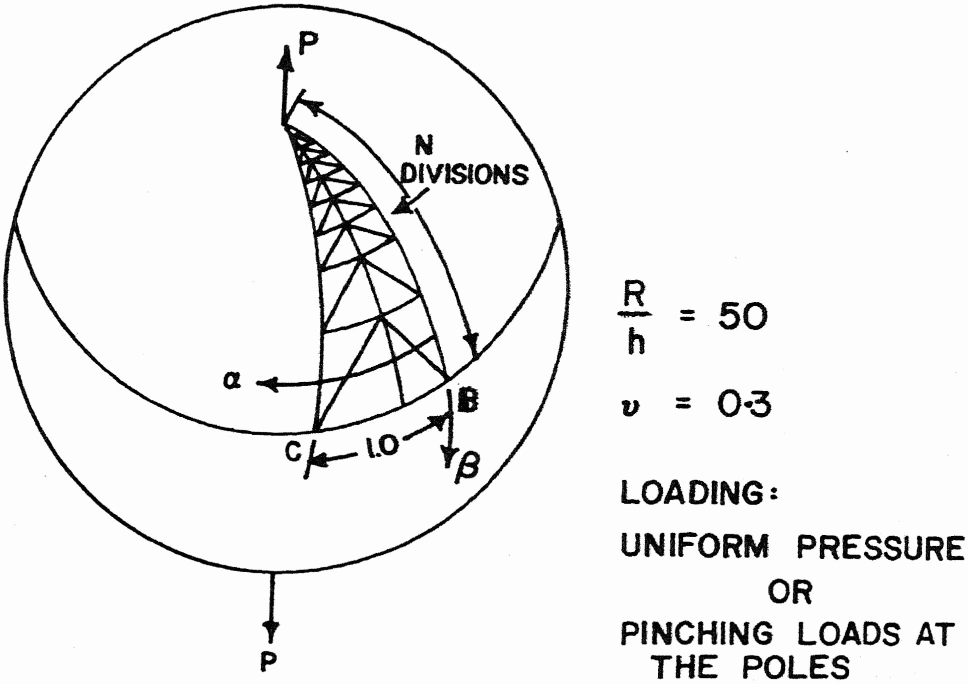

Figure 7 Spherical shell with a typical finite element mesh.

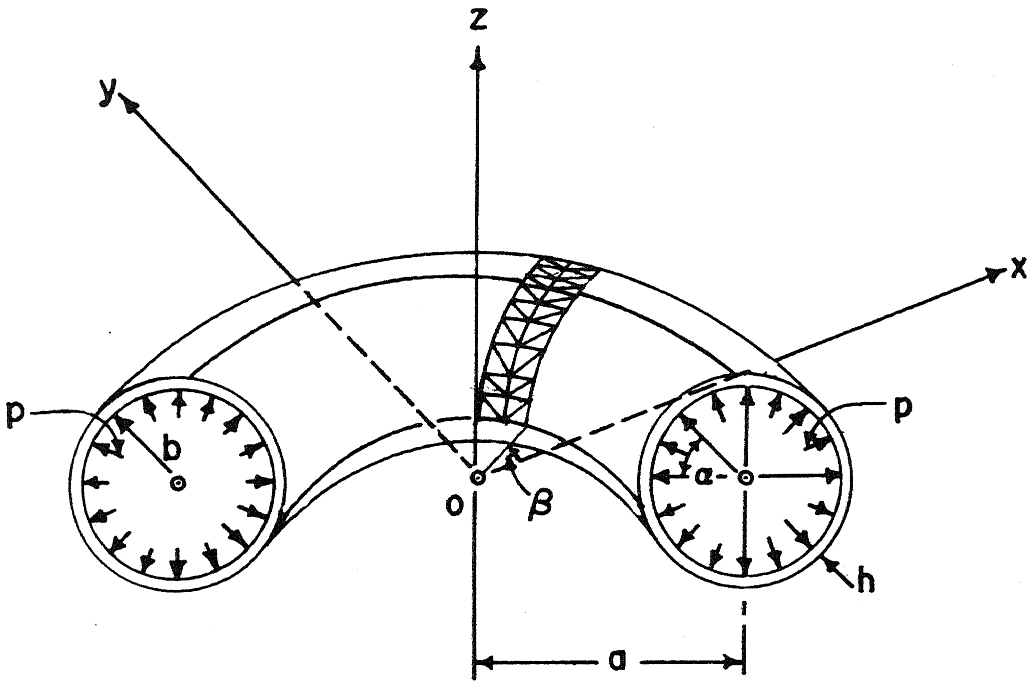

PARAMETRIC EQUATIONS

$$x = (a - b\cos\alpha)\cos\beta$$

$$y = (a - b\sin\alpha)\sin\beta$$

$$z = b\sin\alpha$$

$$\frac{a}{b} = 1{\cdot}5, \quad a = 100\ \text{in}$$

$$\frac{h}{b} = 0{\cdot}05\ \&\ 0{\cdot}005$$

$$\frac{pb}{Eh} = 0{\cdot}002$$

$$\nu = 0{\cdot}3$$

Figure 8 Torus under internal pressure.

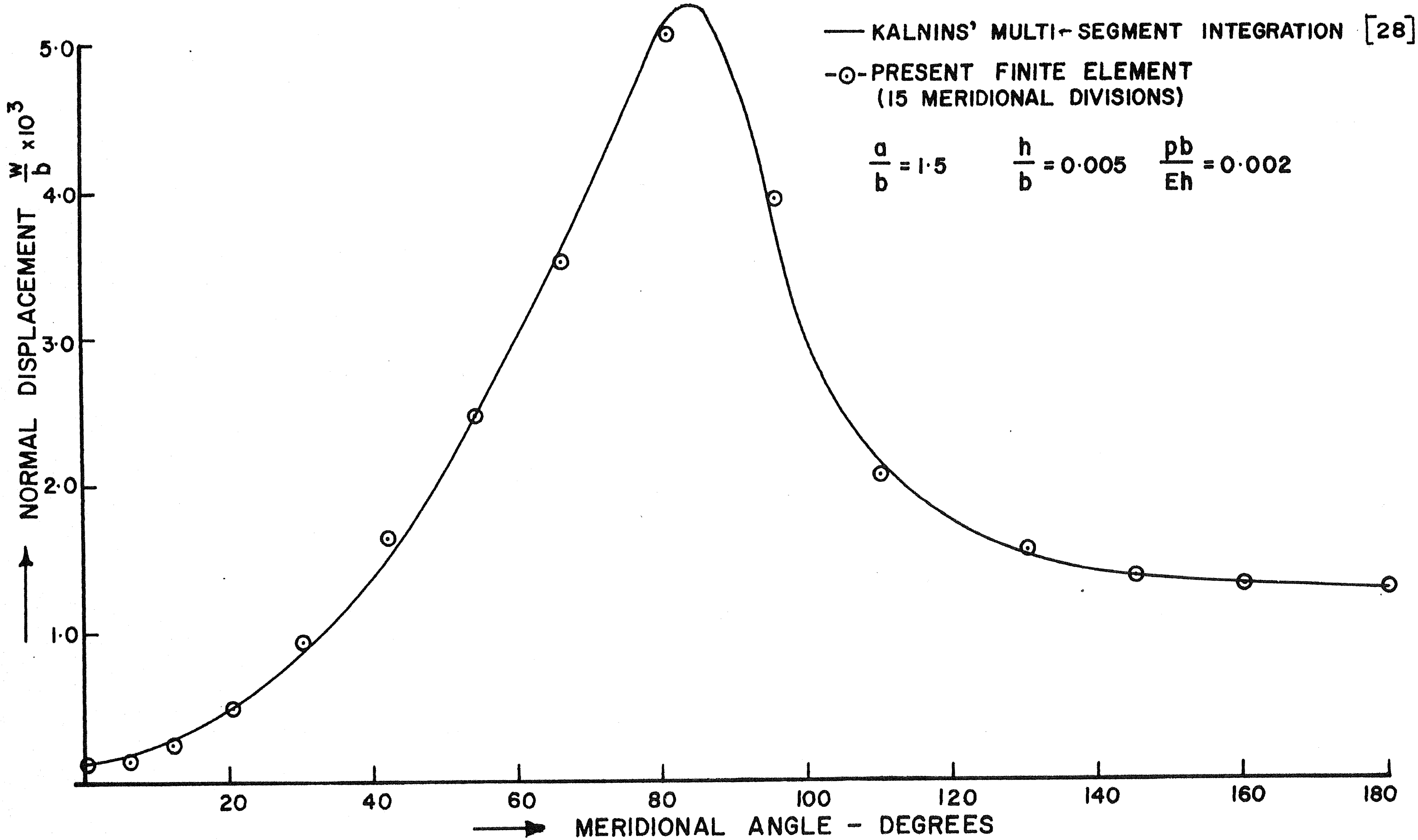

Figure 9 Variation of normal displacement for the torus under internal pressure.

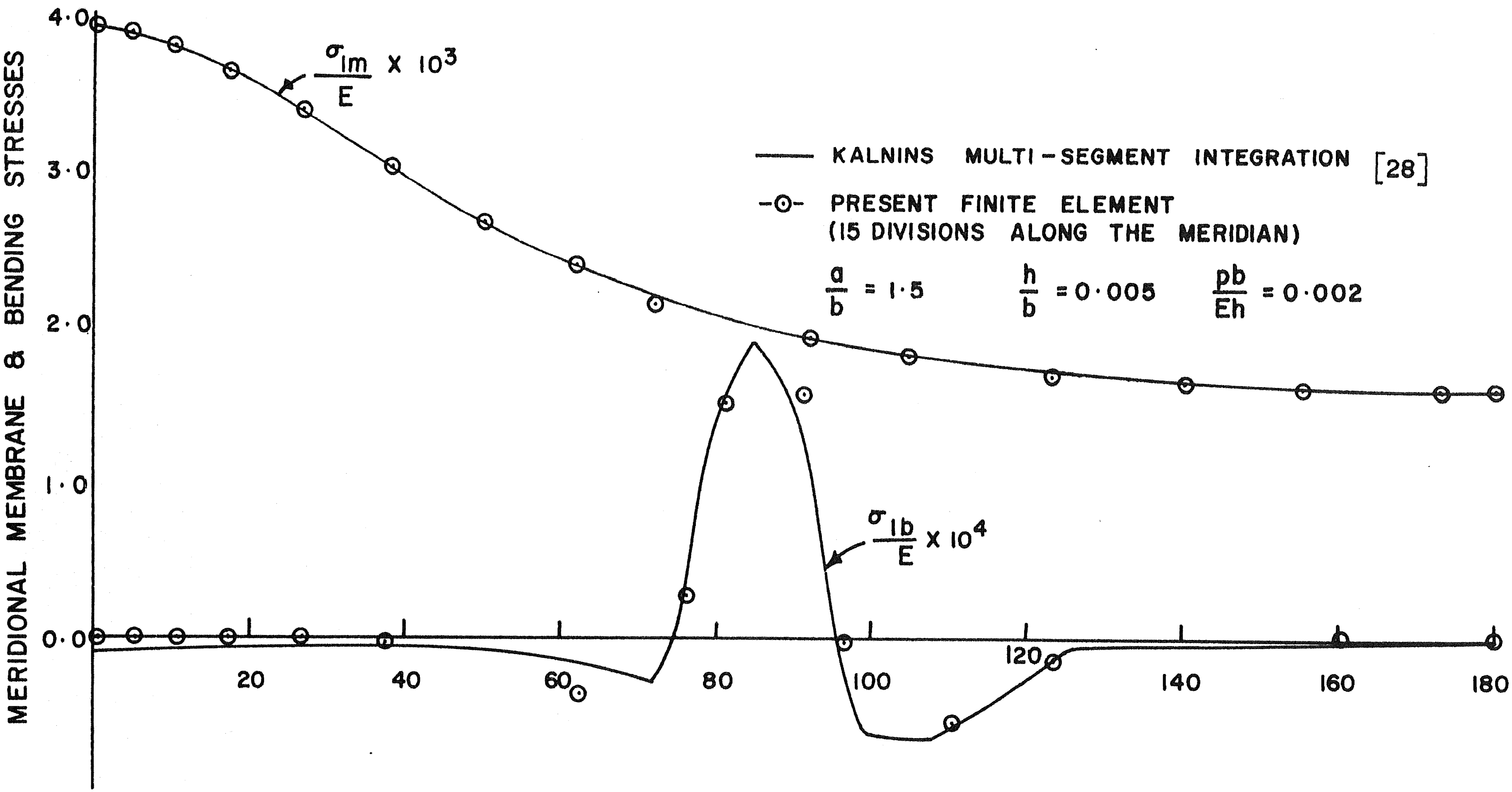

Figure 10 Variation of meridional membrane and bending stresses for the torus under internal pressure.

SS 49

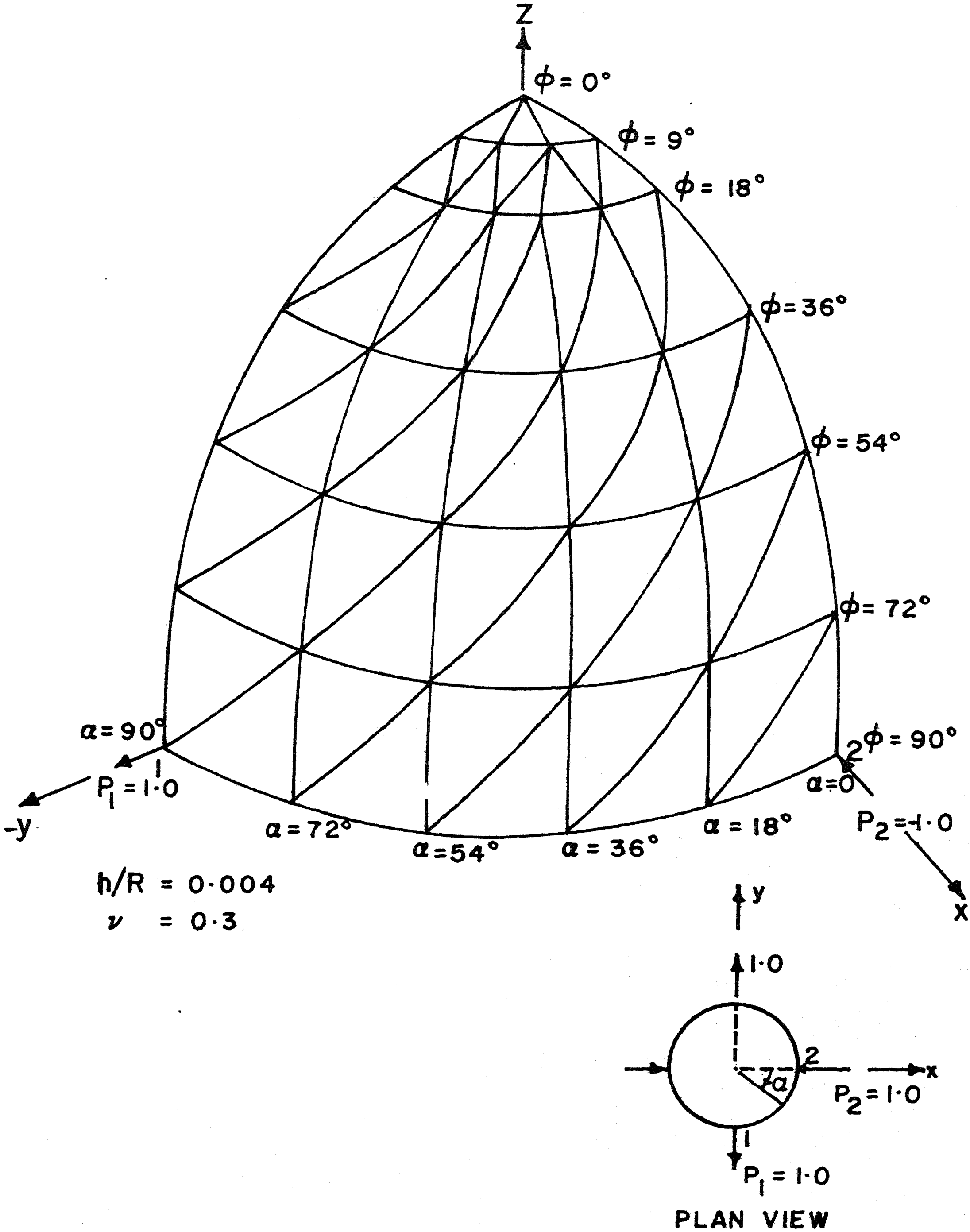

Figure 11 Hemispherical shell subjected to concentrated loads.